Singularities in core-level spectra near metallic surfaces

Despoja, Vito; Šunjić, Marijan; Marušić, Leonardo

Singularities in core-level spectra near metallic surfaces

V. Despoja,* M. Šunjić, and L. Marušić†
Department of Physics, University of Zagreb, Bijenička 32, HR-10000 Zagreb, Croatia
(Received 31 May 2007; revised manuscript received 23 October 2007; published 22 January 2008)

Calculations of the screening shift and dynamical singularity index of the structureless core hole placed near and inside the metallic slab are presented, where the screening mechanism is described using the quantum-mechanical response function calculated in the local density approximation. Core-hole screening shifts show oscillations which are compared with the experimental results. Spatial dependence of the static singularity index, besides experimentally observed enhancement at the surface, shows some new features (bulk oscillations) which were not yet experimentally observed. The dynamical singularity index is used to calculate complete core hole spectrum, including singular line shapes and bulk and surface plasmon losses, and the results explain very well some observed features in the experimental photoemission spectra.

DOI: 10.1103/PhysRevB.77.035424 PACS number(s): 73.20.Mf

I. INTRODUCTION

Spectra of localized levels in solids, e.g., core levels created in x-ray photoemission, show a rich variety of the many-body phenomena, due to their strong interaction with various excitations.[1–14]

Relaxation shifts due to several screening mechanisms,[10–19] chemical shifts,[12,19] satellite peaks due to multiple plasmon or electron-hole pair excitations,[3,6,7] and finally the deviations from the standard line shapes, provide a wealth of information characteristic for specific core levels and their interaction with the environment.[12,14]

It is well known that in metals the excitation of multiple soft electron-hole pairs near the Fermi surface leads to singularities in the low-energy part of the photoelectron spectrum and to the characteristic asymmetric line shapes.[1,4,7] Much theoretical and experimental work has been devoted to study these spectra showing their interesting many-body effects,[9,5] but also in order to determine detailed properties in a variety of systems, as, e.g., their metallic character.

When the core-level photoexcitation occurs near a metallic surface, some new features arise due to the specific character of the screening potentials, so that these effects become spatially dependent. A number of experimental observations and their careful analysis[13–19] since the first experimental observation of this phenomenon[15] confirmed that the singularity index near the surface is enhanced compared to its bulk value.

This problem was theoretically first examined by Kato[3] who calculated the singularity indices $\alpha(\mathbf{R},\omega)$ as functions of frequency ω and core hole position $\mathbf{R}$. Taking the semiclassical approximation and the Thomas-Fermi-type expression for the dielectric screening he obtained a smooth variation of the singularity index, with the enhancement of up to 20% near the surface, as expected from experiments, and its gradual decrease in the vacuum.

In this paper we reconsider this problem, but avoid the approximations made by Kato. The screening mechanism is described using the full quantum-mechanical random phase approximation (RPA) response function calculated with local density approximation (LDA) wave functions for a jellium slab of finite thickness. While confirming the enhancement at the surface obtained by Kato, our results also show interesting oscillatory character of the dynamical singularity index $\alpha(\mathbf{R},\omega)$, which could not be reproduced in the semiclassical approximation.

The knowledge of $\alpha(\mathbf{R},\omega)$ for all ω enables us to evaluate the complete core-hole spectrum. In metals these spectra contain both electron-hole pair excitations, leading to singularities near the elastic line, but also bulk and surface plasmon losses at higher energies.

These two types of losses were usually treated differently, e.g., while high energy losses could be described by expanding the exponent in the spectral function, this could not be done for soft electron-hole pairs. Additional problems arise when one tries to normalize the spectrum because the no-loss line in this case completely disappears.

Recently, Biswas *et al.*[21] performed high precision measurements of core-level photoemission spectra of Al(111), and also presented an extensive review of previous theoretical and experimental work. Their results show many features that indicate the need to describe the whole spectrum in a unified way.

E.g., they had to describe the shape of the plasmon peaks by the so-called asymmetric Lorentzians with widths varying for different experimental parameters, but without providing adequate physical justification. In Sec. IV we therefore calculate the whole core-hole spectrum, by adapting the Minnhagen formula,[6] including finite hole lifetime and proper normalization. The discussion in Sec. IV shows that this approach explains all the main features of the inelastic structures in the experimental spectra of Biswas *et al.*, specifically the plasmon peak asymmetry and its variation with photoelectron direction. Of course, in this analysis one should carefully take into account extrinsic photoelectron scattering and its role in the photoemission processes.

II. FORMULATION OF THE PROBLEM

The Hamiltonian of the system is

$$H = H_0 + H_{int},$$

where

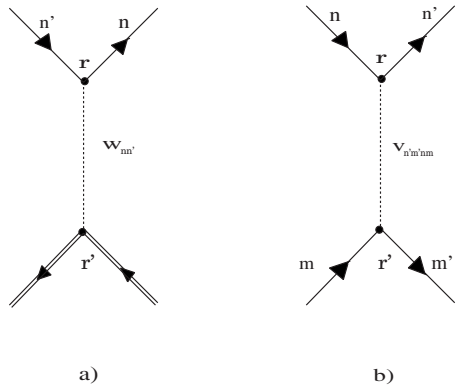

FIG. 1. (a) Hole-electron interaction. (b) Electron-electron interaction.

$$H_0 = E_0 dd^+ + \sum_n E_n c_n^+ c_n$$

describes a (structureless) core hole with unperturbed binding energy $E_0 < 0$, created by the operator d^+, with the wave function localized at $\mathbf{R}$ as follows:

$$u(\mathbf{r} - \mathbf{R}),$$

and the electrons in a metallic slab with energies $E_{n,\mathbf{K}}$ and wave functions

$$\psi_{n,\mathbf{K}}(\mathbf{r}) = e^{i\mathbf{K}\boldsymbol{\rho}} \varphi_n(z),$$

calculated, e.g., in a self-consistent LDA Kohn-Scham scheme (where $\mathbf{K}$ is the component of the wave vector $\mathbf{k}$ parallel to the surface). The interaction contains hole-electron (V_1) and electron-electron (V_2) scattering terms as follows:

$$H_{int} = V_1 + V_2,$$

$$V_1 = d^+ d \sum_{n,n'} w_{nn'} c_n^+ c_{n'},$$

$$V_2 = \sum_{n,n',m,m'} v_{n'm',nm} c_{n'}^+ c_{m'}^+ c_n c_m,$$

where the matrix elements are

$$w_{nn'} = \int d\mathbf{r} \psi_n^*(\mathbf{r}) U(\mathbf{r},\mathbf{R}) \psi_{n'}(\mathbf{r}),$$

$$v_{nn',mm'} = \int d\mathbf{r} d\mathbf{r}' \psi_{n'}^*(\mathbf{r}) \psi_{m'}^*(\mathbf{r}') v(\mathbf{r},\mathbf{r}') \psi_m(\mathbf{r}') \psi_n(\mathbf{r}),$$

with

$$U(\mathbf{r},\mathbf{R}) = \int d\mathbf{r}' v(\mathbf{r},\mathbf{r}') |u(\mathbf{r}' - \mathbf{R})|^2,$$

as shown in Fig. 1. V_1 describes the scattering of the core hole and electrons in the Fermi sea [Fig. 1(a)] (which could, in principle, differ from the bare Coulomb potential) and V_2 describes the electron-electron interaction [$v(\mathbf{r},\mathbf{r}') = e^2/|\mathbf{r} - \mathbf{r}'|$] [Fig. 1(b)].

The core-hole retarded Green's function can be written as

$$G(t) = -i\theta(t) e^{-iE_0 t} \langle d | U(t,0) | d \rangle,$$

where $|d\rangle$ is a one-hole state in a Fermi sea of electrons and $U(t,0)$ is the evolution operator in the interaction representation, or as

$$G(t) = -i\theta(t) e^{-iE_0 t} e^{\Phi(t)}, \quad \Phi(t) = \phi_d(t) + \phi(t). \tag{1}$$

Here the sum of cumulants Φ (Ref. 22) contains $\phi_d(t)$, describing all processes responsible for the core-hole decay (Auger, radiative decay, etc.), and $\phi(t)$ describing the core-hole interaction with the Fermi sea, containing all topologically different connected diagrams of relevant order generated from H_{int}.[22] $\Phi(t)$ can be written in this form because these two mechanisms do not interfere in the lowest order. Also, we can take as a very good approximation,

$$\phi_d(t) = -\gamma t.$$

In the cumulant expansion $\phi(t)$ we shall separate the diagrams where the core hole excites and deexcites charge density fluctuations once, i.e., processes of second order in V_1, and the diagrams of higher order in V_1, where the core hole additionally interacts with the created electron-hole pair, as is shown, e.g., in Fig. 2(a). If we neglect the latter processes, as is the standard approach in the theory of x-ray spectroscopy (XPS) (see, e.g., Refs. 7 and 22) all other cumulants can be summed in a series shown in Fig. 2(b), due to the structureless character of the core hole (no dispersion or recoil). Here Π is the irreducible polarizability including, in principle, all local field corrections. It should be emphasized that, while the neglected class of processes is usually unimportant in XPS, analogous processes are essential for the proper description of x-ray absorption and emission [2,4,7,22] and Auger emission.[8]

If we define the exact response function of the metallic electrons χ (Fig. 3) as the solution of the integral equation

$$\chi(\mathbf{r}_1,\mathbf{r}_2,t_1,t_2) = \prod(\mathbf{r}_1,\mathbf{r}_2,t_1,t_2) + \int d\mathbf{r} d\mathbf{r}' \int dt \prod(\mathbf{r}_1,\mathbf{r},t_1,t) \times v(\mathbf{r},\mathbf{r}') \chi(\mathbf{r}',\mathbf{r}_2,t,t_2),$$

the cumulant sum in Fig. 2(b) can be written as

$$\phi(t) = i \int d\mathbf{r}_1 \int d\mathbf{r}_2 \int_0^t dt_1 \int_0^{t_1} dt_2 U(\mathbf{r}_1,\mathbf{R}) \chi(\mathbf{r}_1,\mathbf{r}_2,t_1,t_2) \times U(\mathbf{r}_2,\mathbf{R}).$$

Introducing the Fourier transform

$$\chi(\mathbf{r}_1,\mathbf{r}_2,t_1,t_2) = \int_{-\infty}^{\infty} \frac{d\omega}{2\pi} e^{-i\omega(t_1 - t_2)} \chi(\mathbf{r}_1,\mathbf{r}_2,\omega),$$

we find

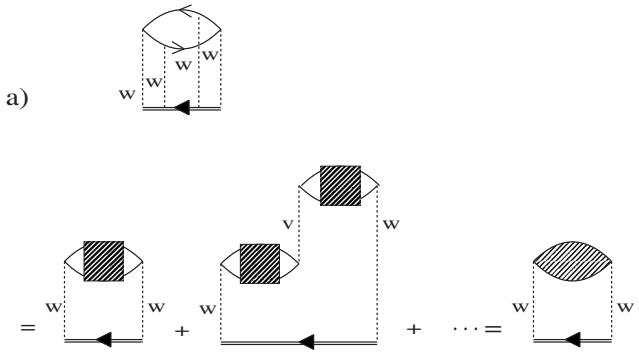

FIG. 2. Cumulant expansion. (a) One of the neglected diagrams of higher order in V_1 (or w). (b) Cumulant sum containing all diagrams of second order in V_1. (c) Irreducible polarizability Π.

$$\phi(t) = -i \int d\mathbf{r}_1 \int d\mathbf{r}_2 U(\mathbf{r}_1,\mathbf{R}) U(\mathbf{r}_2,\mathbf{R}) \times \int_{-\infty}^{\infty} \frac{d\omega}{2\pi} \chi(\mathbf{r}_1,\mathbf{r}_2,\omega) \left\{ \frac{it}{\omega} + \frac{1}{\omega^2}(e^{-i\omega t} - 1) \right\}.$$

If we notice that the induced part of the nonlocal interaction in the Fermi sea can be written as[20]

$$W_{ind}(\mathbf{r},\mathbf{r}',\omega) = \int d\mathbf{r}_1 \int d\mathbf{r}_2 v(\mathbf{r}-\mathbf{r}_1)\chi(\mathbf{r}_1,\mathbf{r}_2,\omega)v(\mathbf{r}_2-\mathbf{r}'),$$

then

$$\phi(t) = -i \int_{-\infty}^{\infty} \frac{d\omega}{2\pi} \int d\mathbf{r} \int d\mathbf{r}' |u(\mathbf{r}-\mathbf{R})|^2 W_{ind}(\mathbf{r},\mathbf{r}',\omega) \times |u(\mathbf{r}'-\mathbf{R})|^2 \left\{ \frac{it}{\omega} + \frac{1}{\omega^2}(e^{-i\omega t} - 1) \right\}.$$

Core-level orbitals are usually small compared to the characteristic screening lengths of metallic electrons, making it appropriate to assume

$$|u(\mathbf{r}-\mathbf{R})|^2 \approx \delta(\mathbf{r}-\mathbf{R}),$$

so that

$$\phi(t) = -i \int_{-\infty}^{\infty} \frac{d\omega}{2\pi} W_{ind}(\mathbf{R},\mathbf{R},\omega) \left\{ \frac{it}{\omega} + \frac{1}{\omega^2}(e^{-i\omega t} - 1) \right\}.$$

For the core hole at the point $\mathbf{R}=(0,0,Z)$ near a surface of the slab which occupies the region $-L<z<0$ (Fig. 4), it is convenient to Fourier transform this result using

$$f(\mathbf{Q},z,z') = \int d\boldsymbol{\rho} e^{i\mathbf{Q}\boldsymbol{\rho}} f(\mathbf{r},\mathbf{r}')$$

to obtain

$$\phi(t) = \int_0^{\infty} d\omega \int \frac{d\mathbf{Q}}{(2\pi)^2} v_Q S(\mathbf{Q},Z,\omega) \left\{ \frac{it}{\omega} + \frac{1}{\omega^2}(e^{-i\omega t} - 1) \right\},$$

where

$$S(\mathbf{Q},Z,\omega) = -\frac{1}{\pi v_Q} \mathrm{Im}\, W_{ind}(Q,Z,Z,\omega), \tag{2}$$

and $v_Q = \frac{2\pi e^2}{Q}$. The core-hole Green's function now becomes

$$G(Z,t) = -i\theta(t) e^{-i[\tilde{E}(Z)-i\gamma]} e^{\tilde{\phi}(Z,t)}, \tag{3}$$

where

$$\tilde{E}(Z) = E_0 + \Delta E(Z).$$

Position dependent shift of the core-hole ground state energy E_0 is

$$\Delta E(Z) = \int_0^{\infty} d\omega \alpha(Z,\omega), \tag{4}$$

where we have defined the new function

$$\alpha(Z,\omega) = \frac{1}{\omega} \int \frac{d\mathbf{Q}}{(2\pi)^2} v_Q S(\mathbf{Q},Z,\omega), \tag{5}$$

which corresponds to the frequency dependent or dynamical singularity index, as will be shown next. The inelastic structures in the spectrum are generated by

$$\tilde{\phi}(Z,t) = \int_0^{\infty} d\omega \frac{\alpha(Z,\omega)}{\omega} \{e^{-i\omega t} - 1\}. \tag{6}$$

Dynamically screened Coulomb interaction

The key quantity that enables us to calculate systematically many-body processes near metallic surfaces is the spa-

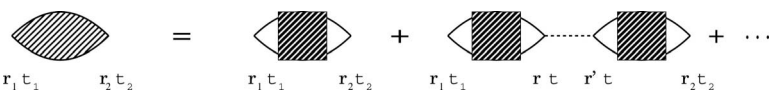

FIG. 3. Response function $\chi(\mathbf{r}_1,\mathbf{r}_2,t_1,t_2)$.

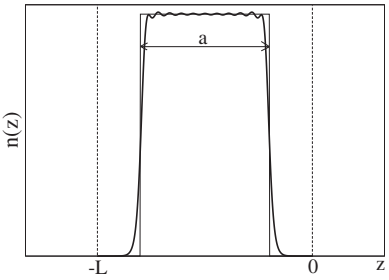

FIG. 4. Metallic slab electron density profile (thick line), positive background of width a (thin line), and electron density edges (dashed lines).

tially dependent response function $\chi(\mathbf{Q},\omega,z,z')$, or its spectral function S, already invoked in Eq. (2), which is related to the induced potential as

$$S(\mathbf{Q},\omega,z,z') = -\frac{1}{\pi v_Q}\,\mathrm{Im}\,W_{ind}(Q,\omega,z,z').$$

Induced Coulomb potential was discussed in detail in Ref. 20. Here we shall need only $W_{ind}(Q,\omega,Z,Z)$ for $Z>0$ and for $-L<Z<0$,

$$W^{p,ind}(\mathbf{Q},Z,Z,\omega) = -v_Q\left\{\frac{c_{-p}\epsilon_p(\mathbf{Q},0,0,\omega)-c_p}{\epsilon_p(\mathbf{Q},0,0,\omega)+1}\right\}e^{-2QZ},\quad Z>0,$$

$$W^{p}(\mathbf{Q},Z,Z,\omega) = v_Q\left\{2\epsilon_p^{-1}(\mathbf{Q},Z,Z,\omega) - \frac{2\epsilon_p(\mathbf{Q},0,0,\omega)}{\epsilon_p(\mathbf{Q},0,0,\omega)+1}\times\epsilon_p^{-1}(\mathbf{Q},Z,0,\omega)\epsilon_p^{-1}(\mathbf{Q},0,Z,\omega)\right\},\quad -L<Z<0,$$

where p denotes the parity and $c_p=1-pe^{-QL}$. $\epsilon_p(\mathbf{Q},z,z',\omega)$ is the $\mathbf{Q}$ component of the nonlocal dielectric function $\epsilon_p(\mathbf{r},\mathbf{r}',\omega)$ defined as

$$\epsilon_p^{-1}(\mathbf{Q},z,z',\omega) = \frac{4Q}{L}\sum_{qq'}\left[\frac{8\pi e^2}{L}\chi^{0p}_{qq'}(\mathbf{Q},\omega) + (Q^2+q^2)\frac{\delta_{qq'}}{\eta_q}\right]^{-1}\cos qz\cos q'z', \quad (7)$$

where $R^{0p}_{qq'}$ is the qq' Fourier component of the free response function.[20]

III. DYNAMICAL SINGULARITY INDEX

In Fig. 5 we show the frequency dependence of the singularity index $\alpha(Z,\omega)$ calculated for several distances Z from the metallic slab. For low ω it is constant, which confirms the validity of the usual approximation, leading to the well-known logarithmic singularity.[1,4,7] Inside the metal ($Z=-20a_0$) $\alpha(Z,\omega)$ is constant over a large energy interval, up to $0.2\omega_s$ ($\approx$2.5 eV for aluminum), and then shows a slight negative slope. At frequencies approaching surface and/or

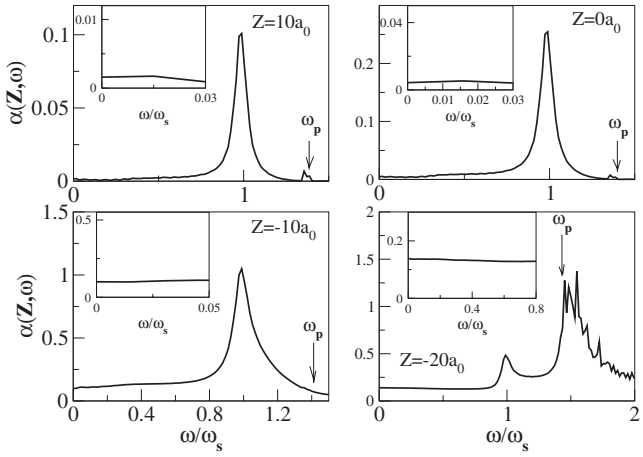

FIG. 5. Frequency dependence of the singularity index $\alpha(Z,\omega)$, for $a=100a_0$, $r_s=2$.

bulk plasmon energies additional structures appear in $\alpha(Z,\omega)$. They generate satellite peaks in XPS, but do not affect the many-body singularity in the low energy part of the spectrum as will be shown in Sec. IV, Figs. 7 and 8. On the contrary, the long tail of the singularity will influence the shape of the higher-energy losses in the spectrum. Dense sharp peaks at frequencies above ω_p are due to strong interband electron-hole transitions from discrete occupied into continuum unoccupied states.

Figure 6 shows the Z dependence of the singularity index $\alpha(Z,0)$. Far from the metallic surface it obviously vanishes, gradually increasing towards the surface, with a maximum slightly inside the surface. It is interesting that the singularity index shows prominent oscillations persisting deep inside the metal. The amplitude of these oscillations increases with r_s, as shown in the inset in Fig. 6.

These oscillations do not appear in the semiclassical approximation for the screening mechanism,[3] where the spatial dependence of the charge density oscillations is neglected. They obviously arise from the Z dependence of the spectral function $S(Q,Z,Z,\omega=0)$ in Eq. (5), but we can analyze them even by considering the unscreened spectral function

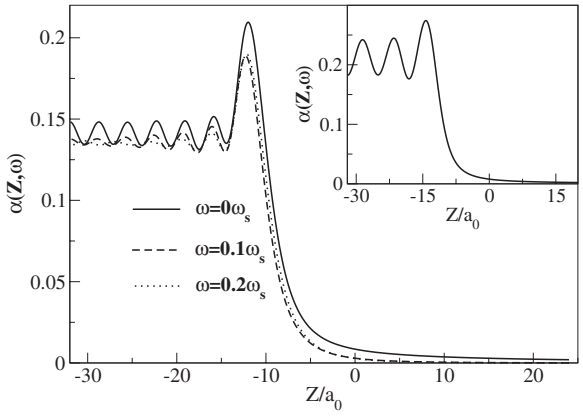

FIG. 6. Spatial dependence of the singularity index $\alpha(Z,\omega)$, for $a=40a_0$, $r_s=2$. The picture in the upper right corner shows the $r_s=4$ case.

$$S_0(\mathbf{Q},Z,\omega=0)=\sum_{n,m,\mathbf{K}}\{f(E_{m,\mathbf{K}+\mathbf{Q}})-f(E_{n,\mathbf{K}})\}$$
$$\times\delta[E_{m,\mathbf{K}+\mathbf{Q}}-E_{n,\mathbf{K}}]\varphi_n^2(Z)\varphi_m^2(Z), \quad (8)$$

which shows the same spatial variation as $\alpha(Z,\omega=0)$. The oscillatory character of the electron density profile, due to the boundary conditions at the surface leads to the similar behavior of the functions S_0, S, and $\alpha(Z,\omega=0)$ as the core-hole position moves inside the solid. Obviously, one could expect the period of these oscillations to be related to k_F, and this indeed turns out to be correct. The absence of these oscillations in Ref. 3 is probably due to the semiclassical approximation for the response function, which neglects the interference terms and has no oscillations in the electron density up to the metallic surface.

IV. CORE-HOLE SPECTRUM

The core-hole spectrum is given by the Green's function (3), i.e., the corresponding spectral function

$$A(Z,\omega)=-\frac{1}{\pi}\,\mathrm{Im}\int_0^\infty dt e^{i[\omega-\tilde{E}(Z)+i\gamma]t}e^{\tilde{\phi}(Z,t)},$$

or

$$A(Z,\omega)=\frac{1}{2\pi}\int_{-\infty}^{\infty}dt e^{i[\omega-\tilde{E}(Z)]t}e^{-\gamma|t|}$$
$$\times\exp\left\{\int_0^\infty d\nu\frac{\alpha(Z,\nu)}{\nu}(e^{-i\nu t}-1)\right\}. \quad (9)$$

This spectrum is obviously normalized

$$\int d\omega A(Z,\omega)=1,$$

and it satisfies the spectral sum rule:[22]

$$\int d\omega\omega A(Z,\omega)=E_0.$$

This means that the average weight of the spectrum remains unchanged, even in the presence of inelastic scattering.

A. Energy shifts

The no-loss line is shifted to higher energies $E_0\rightarrow\tilde{E}(Z)=E_0+\Delta E(Z)$ (because it corresponds to the new ground state of the hole), and in x-ray photoemission the observed electrons excited by photons of frequency ω_0 would have the maximum energy as follows:

$$E_{max}=-|E_0|+\Delta E(Z)+\hbar\omega_0.$$

This energy shift due to the screening of the core hole outside the metal corresponds to the image potential, but with the opposite sign. Figure 7 shows the position of the no-loss line in the photoelectron spectrum, calculated from Eqs. (4) and (5).

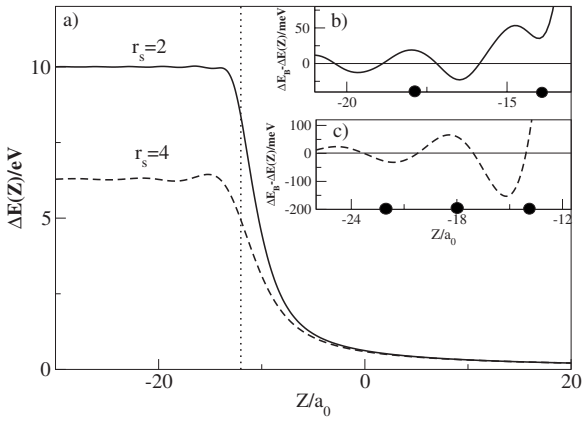

FIG. 7. (a) Core-hole energy shift $\Delta E(Z)$: $r_s=2$ (full line); $r_s=4$ (dashed line). The vertical dotted line represents the jellium edge. [(b) and (c)] Oscillations of the surface core-level shift (SCLS) with amplitudes 75 and 225 meV for $r_s=2$ and 4, respectively. The dots show the approximate positions of the monolayers for (100) orientated surfaces.

Oscillations of the surface core-level shift (SCLS), defined as the difference between the bulk and surface core-hole energy shifts $\Delta E_B-\Delta E(Z)$, where index B denotes the bulk value [i.e., $\Delta E_B=\Delta E(Z\rightarrow-\infty)$], were recently experimentally observed, e.g., for aluminum.[12] The amplitude (difference between first and second monolayer SCLS) of the observed SCLS oscillations for the Al(100) surface is about 100 meV. These shifts are due to a number of mechanisms, but it is interesting to see that even a simple jellium calculation [Figs. 7(b) and 7(c)] produces oscillations which are qualitatively consistent with the experimental results. Figure 7(c) also suggests that SCLS increases with r_s, which was also experimentally evidenced,[16] where for sodium and rubidium SCLS is about 200 meV.

B. Shape of the core-hole spectrum

Normalization of the spectrum is provided for by the factor

$$P_0=\exp\left[-\int_0^\infty\frac{d\omega}{\omega}\alpha(Z,\omega)\right],$$

which gives the intensity of the no-loss or elastic peak. This intensity is reduced because of the appearance of inelastic structures in the spectrum. It is well known[1,4,7,24] that in the case of low-energy electron-hole excitations in the absence of core-hole decay the elastic peak completely disappears, because α is approximately constant up to some cutoff energy D of the order of bandwidth[4]

$$\alpha(\omega)=\alpha(0),\quad \omega<D,$$

as was also confirmed numerically in Sec. III. Therefore we can estimate

$$P_0 \approx \lim_{\epsilon\to 0} \exp\left[-\alpha(Z,0)\int_{\epsilon}^{D}\frac{d\omega}{\omega}\right] = \lim_{\epsilon\to 0}\left(\frac{D}{\epsilon}\right)^{-\alpha(Z,0)} = 0. \tag{10}$$

This indicates that we cannot calculate the inelastic spectrum by expanding the spectral function in Eq. (9) as a power series in the exponent ("satellite generator") $\tilde{\phi}(Z,t)$ in Eq. (9). Therefore we shall use an alternative nonperturbative method to calculate the spectrum including both the low- and high-energy features.

If we neglect extrinsic processes in x-ray photoemission, i.e., scattering of the excited photoelectron in the final state, then the core-hole spectrum corresponds to the observed photoelectron spectrum. This is true only asymptotically, for very high photoelectron energies, but nevertheless could be a reasonable approximation for high excitation energies.

The core-hole spectrum is usually studied separately in the low-energy region, where electron-hole multiple excitations lead to the divergence near the no-loss line, and for larger energies where characteristic (single or even multiple) energy loss peaks occur, due, e.g., to surface and bulk plasmons, ionization losses, etc. If we assume infinite core-hole lifetime ($\gamma\to 0$) and approximate $\alpha=\alpha(Z,\omega=0)$, the photoelectron spectrum would diverge near the elastic line as

$$A(\tilde{\omega}) \sim \tilde{\omega}^{\alpha-1}, \quad \tilde{\omega} = \omega - \tilde{E}(Z). \tag{11}$$

Taking into account finite hole lifetime $\tau=\hbar/\gamma$ in Eq. (1) (which is equivalent to convoluting Eq. (11) with the Lorentzian of width γ), taking again $\alpha=\alpha(Z,\omega=0)$, enables us to derive analytic results for the (non-normalized) spectral function with the asymmetric line shape[1]

$$A_\gamma(\tilde{\omega}) = \frac{\Gamma(1-\alpha)}{(\tilde{\omega}^2+\gamma^2)^{(1-\alpha)/2}}\cos\left\{\frac{\pi\alpha}{2} + (1-\alpha)\arctan\left(\frac{\tilde{\omega}}{\gamma}\right)\right\}, \tag{12}$$

with the maximum at

$$\tilde{\omega}_{max} = \gamma\cot\frac{\pi}{2-\alpha}.$$

Incidentally, this maximum is not the shifted elastic line (which is suppressed in this case) but corresponds to the inelastic structure due to a large number of soft electron-hole pairs. As we move away from the no-loss line and study other inelastic losses we should take into account full $\alpha(Z,\omega)$ dependence, as shown in Fig. 5, for specific core-hole positions Z. Here we have to describe the structures due to collective excitations—surface and bulk plasmons, as well as some particularly strong electron-hole interband transitions (characteristic for a finite slab) that were also observed experimentally.[23]

One might try to describe this higher-energy part of the spectrum by expanding the exponent in Eq. (9),

$$A(Z,\tilde{\omega}) = P_0\frac{1}{2\pi}\int_{-\infty}^{\infty} dt e^{i\tilde{\omega}t}\exp\left\{\int_0^\infty d\nu\frac{\alpha(Z,\nu)}{\nu}e^{-i\nu t}\right\},$$

leading to

$$A(Z,\tilde{\omega}) = P_0\delta(\tilde{\omega}) + P_0\frac{\alpha(Z,\tilde{\omega})}{\tilde{\omega}} + \cdots. \tag{13}$$

However, as mentioned before, the no-loss term vanishes because of $P_0\to 0$, but this also complicates the interpretation of the second and other terms in Eq. (13), corresponding to single and multiple losses. It is therefore necessary to calculate a complete spectrum with full $\alpha(Z,\tilde{\omega})$, without resorting to the expansion in Eq. (13). We shall do it by using a modification of the Minnhagen method.[6] From Eqs. (3) and (6) we can prove that the core-hole Green's function satisfies the equation

$$\left\{i\frac{\partial}{\partial t} - \tilde{E}(Z) + i\gamma\right\}G(Z,t) = \delta(t) + G(Z,t)\int_0^\infty d\nu\alpha(Z,\nu)e^{-i\nu t}.$$

After Fourier transformation we obtain an integral equation for Green's function, which can be separated into real and imaginary parts G_R and G_I, respectively.

$$G_R(Z,\tilde{\omega}) = G_{0R}(Z,\tilde{\omega})[1+J_R(Z,\tilde{\omega})] - G_{0I}(Z,\tilde{\omega})J_I(Z,\tilde{\omega}), \tag{14}$$

$$G_I(Z,\tilde{\omega}) = G_{0I}(Z,\tilde{\omega})[1+J_R(Z,\tilde{\omega})] + G_{0R}(Z,\tilde{\omega})J_I(Z,\tilde{\omega}), \tag{15}$$

where

$$J_{R,I}(Z,\tilde{\omega}) = \int_0^\infty d\nu\alpha(Z,\nu)G_{R,I}(Z,\tilde{\omega}-\nu),$$

and

$$G_{0R}(\tilde{\omega}) = \frac{\tilde{\omega}}{\tilde{\omega}^2+\gamma^2}, \quad G_{0I}(\tilde{\omega}) = -\frac{\gamma}{\tilde{\omega}^2+\gamma^2}. \tag{16}$$

Equations (14) and (15) can be solved by using the iterative procedure which starts with G_0 given by Eq. (16). For $\alpha(\omega)=\alpha(0)$, one immediately obtains the Doniach-Šunjić (DS) form (12). Figure 8 shows the core-hole spectra calculated from

$$A(Z,\tilde{\omega}) = -\frac{1}{\pi}G_I(Z,\tilde{\omega}), \tag{17}$$

with G_I obtained self-consistently from Eqs. (14) and (15), and for the singularity index $\alpha(Z,\nu)$ calculated from Eq. (5) for several Z.

This method enables us to calculate the whole normalized spectrum, but we shall first analyze the strength of the no-loss peak, i.e., the $\tilde{\omega}=0$ pole contribution to the spectrum in the Lorentzian form

$$A_0(Z,\tilde{\omega}) = \frac{\gamma}{\tilde{\omega}^2+\gamma^2}.$$

From Eq. (15) one finds

$$A(Z,\tilde{\omega}\to 0) \to Z(\gamma)A_0(\tilde{\omega})$$

for the decay constant γ, where $Z(\gamma)$ is the strength of the residuum,

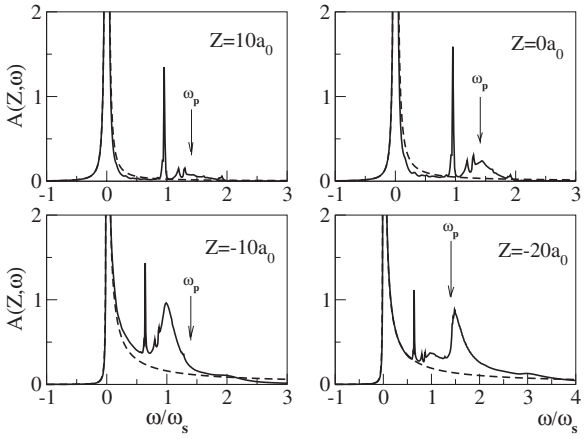

FIG. 8. Full lines represent the core-hole spectra for various hole positions inside and outside the metallic slab ($a=50a_0$ and $r_s=2$); dashed lines are the appropriate DS line shapes. Core-hole decay constant is $\gamma=0.002\omega_S$.

$$Z(\gamma) = 1 + J_R(Z, \tilde{\omega} = 0),$$

or alternatively,

$$Z(\gamma) = \pi\gamma A(Z, \tilde{\omega} = 0).$$

Figure 9 shows the γ dependence of the no-loss peak in the spectrum. For $\gamma \to 0$ it disappears, which is in agreement with Eq. (10) but for finite γ it reappears as an appreciable contribution to the spectrum, as can be also seen in Fig. 10.

For larger distances ($Z=10a_0$) Fig. 8 shows that the low-energy part is almost symmetrical, except for a slight distortion due to even surface plasmons (sharp peak below ω_S). Symmetry of the elastic line is expected because electron-hole excitations contribute only slightly outside the surface. In the surface region ($Z=0,-10a_0$) odd surface plasmon peak becomes pronounced. Also, asymmetry due to electron-hole excitations becomes visible, which is even more obvious from the appropriate DS line shapes. Inside the slab ($Z=-20a_0$) bulk plasmon losses (peak around $\omega \approx \sqrt{2}\omega_S$) begin to dominate. At and inside the multiple surface plasmon

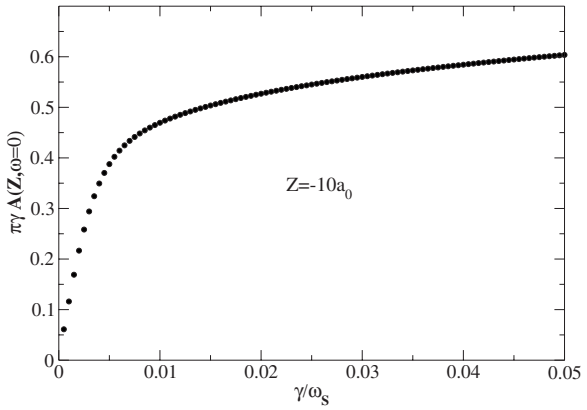

FIG. 9. γ dependence of the strength of the no-loss peak. $Z=-10a_0$.

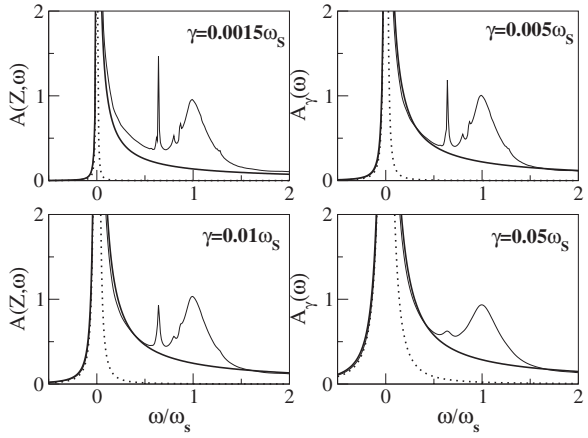

FIG. 10. Core-hole spectra for various core-hole lifetimes γ (thin lines); thick lines represent the corresponding DS line shapes. The core-hole position is $Z=-10a_0$, $a=50a_0$, and $r_s=2$.

losses are also visible, e.g., weak maxima around $\omega=2\omega_S$ and $\omega=3\omega_S$ for $Z=-10a_0$ and $Z=-20a_0$, respectively. The core-hole decay constant is taken to be $\gamma=0.002\omega_S \approx 23$ meV which is consistent with experimentally measured value 23 ± 5 meV.[12]

Figure 10 shows core-hole spectra for various decay constants γ and a fixed position ($Z=-10a_0$). For $\gamma=0.0015\omega_S$ the spectrum shows characteristic $\omega^{\alpha(0)-1}$ shape corrected by the two surface plasmon peaks. For larger γ, spectra are very similar to the DS line shape almost in all energy range except for inelastic losses around ω_S. The no-loss peak is shown by the dotted line, which for $\tilde{\omega}<0$ is identical to the full line of the total spectrum. One notices the growth of the elastic contribution in the spectrum with γ.

C. Discussion of the plasmon losses

Now we shall briefly analyze how our calculated core-hole spectra compare with the measured photoemission spectra. In this analysis one should take into account the role of the extrinsic processes, i.e., the photoelectron scattering in the final state, as well as the interference between photoelectron and hole scattering. These extrinsic processes introduce angular and photon energy dependence of the spectra and limit the photoelectron escape depth.

Extrinsic scattering is minimal for the normal photoemission, so the photoelectron spectrum can be approximated by the core-hole spectrum. In Fig. 1 of Ref. 21 we indeed observe this behavior with the striking similarity to the spectrum calculated in our Fig. 8 for $Z=-20a_0$, containing asymmetric main line, weak surface, and strong bulk plasmons. At a nearly grazing angle the escape depth is reduced, and the experimental spectrum resembles our calculations (Fig. 8) for $Z=-10a_0$.

Figure 2 of Ref. 21 shows systematically this variation of Al $2s$ and $2p$ lines with angle, which corresponds to the varying importance of extrinsic scattering both in reducing escape depth and contributing to the inelastic spectrum. It should be noted that extrinsic scattering contributes to the strength of the plasmon peaks, but not to the electron-hole

excitations near the main peak. However, it influences the asymmetry of the plasmon peaks indirectly. Namely, the intrinsically excited plasmons are asymmetrical as shown in our calculated spectra and confirmed in experiment, because they contain information about the singular electron-hole part of the spectrum, but extrinsically excited plasmons are not. For increasing exit angle the ratio of those two contributions to the plasmon peaks changes, the intrinsic one decreasing, and the peaks become more Lorentzian-like.

This discussion, in fact, agrees completely with the explanation given by Biswas *et al.*,[21] who also quantify it in terms of the left and right Lorentzian widths used to fit the plasmon peaks. However, we cannot only confirm it but also explain the physical origin of this asymmetry in the intrinsically excited plasmons and calculate their spectral shapes. More detailed quantitative analysis of the experiments would require proper theoretical inclusion of the extrinsic scattering, but even this qualitative discussion confirms the results of our theoretical treatment of the hole interaction with the soft electron-hole pairs and high-energy plasmons near surfaces, including the calculation of the whole spectrum within the same formalism.

V. CONCLUSION

We have analyzed qualitatively and quantitatively the dynamical screening of the core hole near a metallic surface as observed in the photoelectron spectra. The obtained results confirm the expected behavior of the screening mechanism, specifically the transition from the surface to bulk screening, e.g., enhanced static singularity index or surface core-level shift. Dynamical singularity index is used in the self-consistent equation for the Green's function to calculate the complete core-hole spectral function, including the standard low-energy DS line shape, and multiple surface and bulk plasmon satellites. Comparison with available experimental results confirms that the calculated core-hole spectra qualitatively explain the observed trends in the photoemission spectra, in particular, the shape of the main singular peak and plasmon satellites.

*Email address: vito@phy.hr
†Present address: Department of Transport and Maritime Studies, University of Zadar, M. Pavlinovića, HR-23000 Zadar, Croatia.

[1] S. Doniach and M. Šunjić, J. Phys. C **3**, 285 (1969).
[2] P. Nozieres and C. T. de Dominicis, Phys. Rev. **178**, 1097 (1969).
[3] Masahiko Kato, Phys. Rev. B **38**, 10915 (1988).
[4] E. Muller-Hartman, T. V. Ramakrishnan, and G. Toulouse, Phys. Rev. B **3**, 1102 (1971).
[5] G. D. Mahan, Phys. Rev. B **25**, 5021 (1982).
[6] P. Minnhagen, Phys. Lett. **56A**, 327 (1976).
[7] D. C. Langreth, Phys. Rev. B **1**, 471 (1970).
[8] M. Natta and P. Joyes, J. Phys. Chem. Solids **31**, 447 (1970).
[9] J. A. Leiro and M. H. Heinonen, Phys. Rev. B **59**, 3265 (1999).
[10] D. M. Riffe, G. K. Wertheim, and P. H. Citrin, Phys. Rev. Lett. **63**, 1976 (1989).
[11] D. M. Riffe, W. Hale, B. Kim, and J. L. Erskine, Phys. Rev. B **51**, 11012 (1995).
[12] M. Borg, M. Birgersson, M. Smedh, A. Mikkelsen, D. L. Adams, R. Nyholm, C. O. Almbladh, and J. N. Andersen, Phys. Rev. B **69**, 235418 (2004).
[13] A. Baraldi, S. Lizzit, A. Novello, G. Comelli, and R. Rosei, Phys. Rev. B **67**, 205404 (2003).
[14] D. M. Riffe and G. K. Wertheim, Phys. Rev. B **61**, 2302 (2000).
[15] P. H. Citrin, G. K. Wertheim, and Y. Baer, Phys. Rev. B **16**, 4256 (1977).
[16] G. K. Wertheim, D. M. Riffe, and P. H. Citrin, Phys. Rev. B **45**, 8703 (1992).
[17] Bongsoo Kim and Kwang Joo Kim, J. Korean Phys. Soc. **30**, 83 (1996).
[18] M. Zacchigna, C. Astaldi, K. C. Prince, M. Sastry, C. Comicioli, M. Evans, R. Rosei, C. Quaresima, C. Ottaviani, C. Crotti, M. Matteucci, and P. Perfetti, Phys. Rev. B **54**, 7713 (1996).
[19] P. H. Citrin, G. K. Wertheim, and Y. Baer, Phys. Rev. B **27**, 3160 (1983).
[20] L. Marušić and M. Šunjić, Phys. Scr. **63**, 336 (2001).
[21] C. Biswas, A. K. Shukla, S. Banik, V. K. Ahire, and S. R. Barman, Phys. Rev. B **67**, 165416 (2003).
[22] G. D. Mahan, *Many-Particle Physics*, 2nd ed. (Pergamon, New York, 1990).
[23] M. Rocca, M. Lazzarino, and U. Valbusa, Phys. Rev. Lett. **69**, 2122 (1992); L. Savio, L. Vattuone, and M. Rocca, Phys. Rev. B **61**, 7324 (2000); G. Chiarello, V. Formoso, A. Santaniello, E. Colavita, and L. Papagno, *ibid.* **62**, 12676 (2000).
[24] P. W. Anderson, Phys. Rev. Lett. **18**, 1049 (1967).